Electronic Supplementary Material (ESI) for Physical Chemistry Chemical Physics.
This journal is © the Owner Societies 2019

Electronic Supplementary Information

Structure and sum-frequency generation spectra of water on uncharged Q_4 silica surfaces: a molecular dynamics study

Konstantin S. Smirnov*

Univ. Lille, CNRS, UMR 8516 – LASIR – Laboratoire de Spectrochimie Infrarouge et Raman, F-59000 Lille, France

1 Dipole and polarizability models

1.1 Dipole and polarizability of water slab

The dipole **M** and polarizability **A** of a system of water molecules were obtained as the sum of corresponding molecular quantities

$$\mathbf{M} = \sum_i \boldsymbol{\mu}_i \tag{S1}$$

$$\mathbf{A} = \sum_i \mathbf{a}_i \tag{S2}$$

with $\boldsymbol{\mu}_i$ and $\mathbf{a}_i$ denoting the dipole moment and polarizability tensor of molecule i, respectively. The effect of intermolecular interactions in condensed phase was taken into account with dipole interaction model.[1,2] In a system of N interacting molecules that are characterized by permanent dipoles $\boldsymbol{\mu}^0$ and polarizability tensors $\boldsymbol{\alpha}$, the dipole $\boldsymbol{\mu}_i$ of molecule i is given by

$$\boldsymbol{\mu}_i = \boldsymbol{\mu}_i^0 + \boldsymbol{\alpha}_i \big(\boldsymbol{\mathcal{E}}_i^0 + \sum_{j \neq i} \hat{T}_{ij} \boldsymbol{\mu}_j\big), \tag{S3}$$

where $\boldsymbol{\mathcal{E}}_i^0$ is an external electric field at the molecule's position $\mathbf{r}_i$ and $\hat{T}_{ij}$ is the dipole-dipole interaction tensor

$$\hat{T}_{ij} = \frac{1}{r_{ij}^3}\big(3\mathbf{e}_{ij}\mathbf{e}_{ij}^T - \mathbf{1}\big) \tag{S4}$$

with $\mathbf{e}_{ij} = \mathbf{r}_{ij}/r_{ij}$ ($\mathbf{r}_{ij} = \mathbf{r}_i - \mathbf{r}_j$) and $\mathbf{1}$ being an unit matrix. The set of N equations (S3) can be rewritten in a matrix form

$$\mathbf{m} = \mathbf{m}^0 + \mathbf{a}\big(\mathbf{E}^0 + \mathbf{Tm}\big) = \mathbf{m}^0 + \mathbf{aE}, \tag{S5}$$

where $\mathbf{E} = \mathbf{E}^0 + \mathbf{Tm}$. The formal solution of (S5) for $\mathbf{E}$ reads

$$\mathbf{E} = \big(\mathbf{1} - \mathbf{Ta}\big)^{-1}\big(\mathbf{E}^0 + \mathbf{Tm}_0\big) \tag{S6}$$

and therefore, one obtains the vector of dipoles $\mathbf{m}$ as

$$\mathbf{m} = \mathbf{m}^0 + \mathbf{a}(\mathbf{1} - \mathbf{Ta})^{-1}(\mathbf{E}^0 + \mathbf{Tm}_0) = \mathbf{m}^0 + \mathbf{a}^{\mathrm{eff}}(\mathbf{E}^0 + \mathbf{Tm}_0), \tag{S7}$$

---

*E-mail: konstantin.smirnov@univ-lille.fr where $\mathbf{a}^{\text{eff}} \equiv \mathbf{a}(\mathbf{1} - \mathbf{Ta})^{-1}$ is a $3N \times 3N$ matrix of effective system polarizability. The dipole $\boldsymbol{\mu}_i$ of molecule i is readily available from (S7), whereas the polarizability tensor $\mathbf{a}_i$ is given by[2]

$$\mathbf{a}_i = \sum_j \mathbf{a}_{ij}^{\text{eff}}, \tag{S8}$$

where the sum runs over 3×3 blocks of the matrix $\mathbf{a}^{\text{eff}}$.

1.2 Dipole and polarizability models for water molecule

The dipole $\boldsymbol{\mu}_i^0$ and polarizability $\boldsymbol{\alpha}_i$ of an isolated water molecule were obtained with models based on those proposed by Morita and Hynes[2].

Dipole model. Dipole of a molecule is computed as

$$\boldsymbol{\mu}^0 = \sum_k q_k \mathbf{r}_k \tag{S9}$$

where q_k and $\mathbf{r}_k$ denote the charge and position vector of atom k, respectively. In order to reproduce changes of $\boldsymbol{\mu}^0$ upon the dynamics of atoms, the atomic charges q_k were made geometry-dependent. Following ref. 2, the variation charge Δq_i of each of the two hydrogen atoms (i = 1, 2) is written in the form

$$\Delta q_i \equiv q_i - q_{\text{H}}^0 = a\Delta R_i + b\Delta R_i^2 + c\Delta\theta + d\Delta\theta^2 + e\Delta R_i \Delta R_j + f\Delta R_i \Delta\theta, \tag{S10}$$

where q_{H}^0 is the charge in the equilibrium geometry, ΔR and θ are deviations of OH bond length and HOH angle θ from their equilibrium values, respectively, and a, b, c, d, e, f are coefficients.

By using symmetry-adapted internal coordinates

$$S_1 = \Delta R_1 + \Delta R_2,\; S_2 = \Delta R_1 - \Delta R_2 \text{ and } S_3 = \Delta\theta \tag{S11}$$

to describe variations of molecular geometry, one can obtain the following expressions for symmetry-adapted variations of Δq_i

$$\Delta q_1 + \Delta q_2 = C_1 S_1 + C_2 S_1^2 + C_3 S_2^2 + C_4 S_3 + C_5 S_3^2 + C_6 S_1 S_3 \tag{S12}$$

$$\Delta q_1 - \Delta q_2 = C_7 S_2 + C_8 S_1 S_2 + C_9 S_2 S_3 \tag{S13}$$

$$\Delta q_{\text{O}} = -\left(\Delta q_1 + \Delta q_2\right), \tag{S14}$$

with the neutrality fulfilled. Then, using q_{H}^0 and combinations (S12)-(S14), it is straightforward to recover the charges q_k necessary for computing the dipole $\boldsymbol{\mu}_i^0$ (S9).

Polarizability model. The polarizability of water molecule was described by a bond polarizability model that represents polarizability tensor $\boldsymbol{\alpha}$ of molecule in Cartesian frame as the sum of bond polarizabilities

$$\boldsymbol{\alpha} = \sum_i \boldsymbol{\pi}_i, \tag{S15}$$

where the bond polarizability tensor $\boldsymbol{\pi}_i$ of OH bond i (i = 1, 2) is given by

$$\boldsymbol{\pi}_i = \mathbf{U}_i \, \mathbf{p}_i \, \mathbf{U}_i^{-1}. \tag{S16}$$

Table S1: Coefficients in eqns (S12), (S13) and (S18) (in au, rad^{-1}, rad^{-2}) for describing the dependence of atomic charges and OH bond polarizability tensor components on the geometry of water molecule.

Dipole model parameters								
C_1	C_2	C_3	C_4	C_5	C_6	C_7	C_8	C_9
-0.13583	0.01507	0.02879	0.12088	0.05638	-0.05557	-0.06824	0.01472	0.11277
Polarizability model parameters								
P_1	P_2	P_3	P_4	P_5				
5.63841	7.24435	3.53273	1.00417	2.90802				
P_6	P_7	P_8						
4.80441	1.69457	0.34341						
P_9	P_{10}	P_{11}	P_{12}					
4.62814	0.69777	0.64988	-2.22892					

In (S16), $\mathbf{U}_i$ stands for a rotation matrix transforming the bond polarizability tensor $\mathbf{p}_i$ in its principal coordinates to the tensor $\boldsymbol{\pi}_i$ in the Cartesian frame. The tensor $\mathbf{p}_i$ has the following form

$$\mathbf{p}_i = \begin{pmatrix} p_{i,L} & & \\ 0 & p_{i,T1} & \\ 0 & 0 & p_{i,T2} \end{pmatrix}, \tag{S17}$$

where the subscripts L, $T1$ and $T2$ denote the longitudinal and two transversal axes of the bond polarizability tensor, respectively; the longitudinal axis is directed along the OH bond and the first transversal axis is perpendicular to the molecular plane. Dependence of the three non-zero components of $\mathbf{p}_i$ on the internal coordinates was described with the following functional forms

$$\begin{aligned} p_{i,L} &= P_1 + P_2\Delta R_i + P_3\Delta R_i^2 + P_4\Delta R_j + P_5\Delta R_i\Delta R_j \\ p_{i,T1} &= P_6 + P_7\Delta R_i + P_8\Delta\theta \\ p_{i,T2} &= P_9 + P_{10}\Delta R_i + P_{11}\Delta\theta + P_{12}\Delta R_i\Delta R_j. \end{aligned} \tag{S18}$$

Model parameters and model performance. The coefficients in eqns (S12), (S13) and (S18) were derived by fitting model atomic charges and molecular polarizabilities to reference values obtained in quantum-chemical calculations. For this purpose, geometry of an isolated water molecule was randomly varied in the limits $R_{\mathrm{OH}} = (R^0_{\mathrm{OH}} - 0.1\,\text{Å}, R^0_{\mathrm{OH}} + 0.2\,\text{Å})$ and $\theta = (\theta_0 - 6^\circ, \theta_0 + 12^\circ)$ and ESP atomic charges and molecular polarizabilities were computed for a total of 300 configurations. The calculations used Gaussian09 code and were performed at the DFT level with the B3LYP exchange-correlation functional and pVTZ basis set by Sadlej[3] that has been specifically designed to reproduce molecular dipoles and polarizabilities. The equilibrium value of hydrogen charge is equal to $q^0_{\mathrm{H}} = 0.3277\ |e|$.

Values of the coefficients obtained in the least squares fits are reported in Table S1. Figure S1 illustrates the performance of the dipole and polarizability models. The former perfectly mimics changes of molecular dipole upon variation of molecular geometry. The latter also gives a very good agreement between the fitted and reference values of four non-zero components of the polarizability tensor; the majority of absolute relative errors for the polarizability tensor elements is smaller than 0.5 %. It should be noted that alternative functional forms for the polarizability tensor elements (S18) were tested, but they did not result in a notable improvement of the fit quality. Judging on the results presented in Figure S1, the quality of the dipole model is comparable with that used in ref. 2, while the polarizability model yields a better agreement between the model and reference quantities than such a model developed in ref. 2 (*cf.* Fig. 1, ref. 2).

Assessment of the model performance for the spectral intensity calculations was done by computing the infrared absorption coefficient and Raman activity of the vibrational modes. The dipole and polarizability

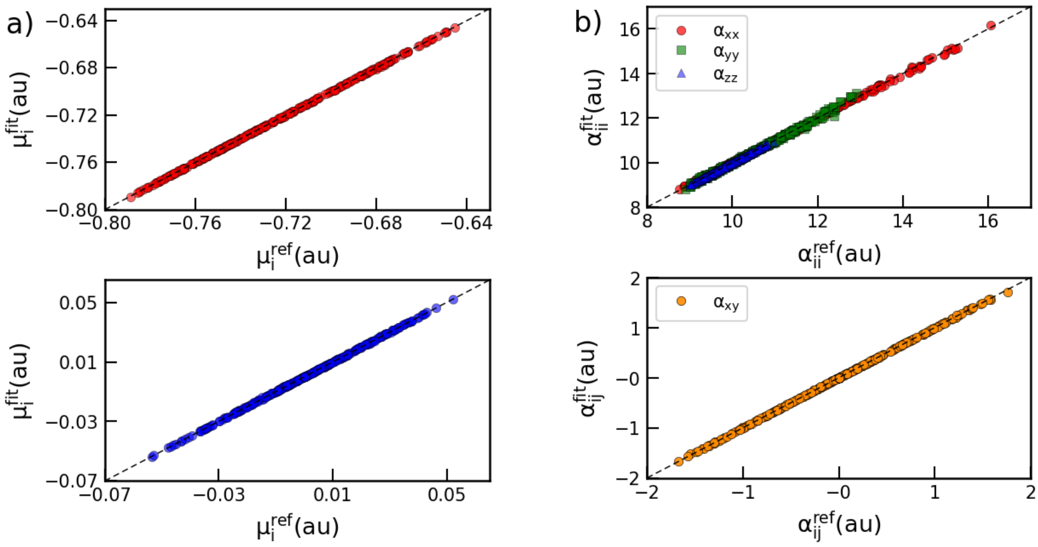

Figure S1: Correlations between the reference and model values of the non-zero dipole components (a), and of the non-zero elements of the polarizability tensor (b) in a total of 300 geometries of water molecule. Dashed line in the plots denotes the identity line.

tensor derivatives entering these quantities were obtained by the finite difference method using Cartesian vectors of atomic displacements in the vibrational modes. Figure S2 compares the spectral intensities yielded by the models with their counterparts obtained by the DFT calculations. The agreement is excellent in all cases, except the Raman activity of the angle-bending mode for which the polarizability model underestimates the activity by *ca.* 25 %. The reason for such a large error lies in the fact that the activity of the mode primarily comes from the anisotropy of the polarizability tensor derivative which has non-zero diagonal elements for this mode. As the anisotropy depends on difference between these elements, the relative error is amplified that, in its turn, causes a high relative error for this mode of low Raman activity.

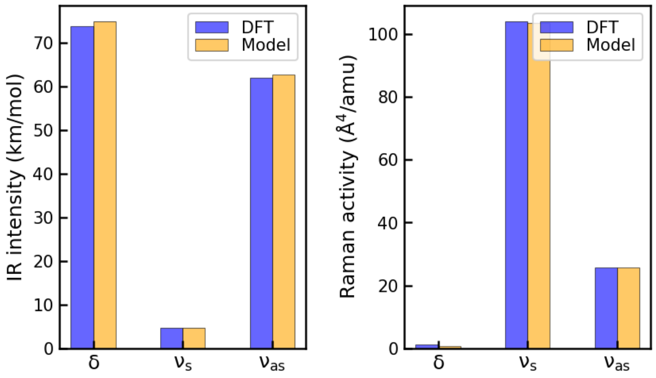

Figure S2: Comparison of infrared absorption coefficients (left) and Raman activities (right) of the vibrational modes of water molecule obtained in the DFT calculations and computed with the dipole and polarizability models; δ, ν_s and ν_{as} denote angle-bending, symmetric bond-stretching and asymmetric bond-stretching modes, respectively.

Finally, the models were tested by computing the dipole and polarizability variations in the vibrational modes of water molecule beyond the harmonic approximation. For this purpose, the atoms of H_2O molecule were displaced along the vectors of atomic displacements with large amplitudes. The variations of non-zero components of the dipole and polarizability tensor are compared with reference DFT values in Figure S3 and Figure S4 for the symmetric and asymmetric bond-stretching modes, respectively. The behaviour of the quantities is confidently reproduced at small and intermediate displacement amplitudes, but the agreement worsens when the amplitude increases. Nevertheless, the relative errors are small and the dipole and polarizability models have the quality sufficient for the purpose of the work.

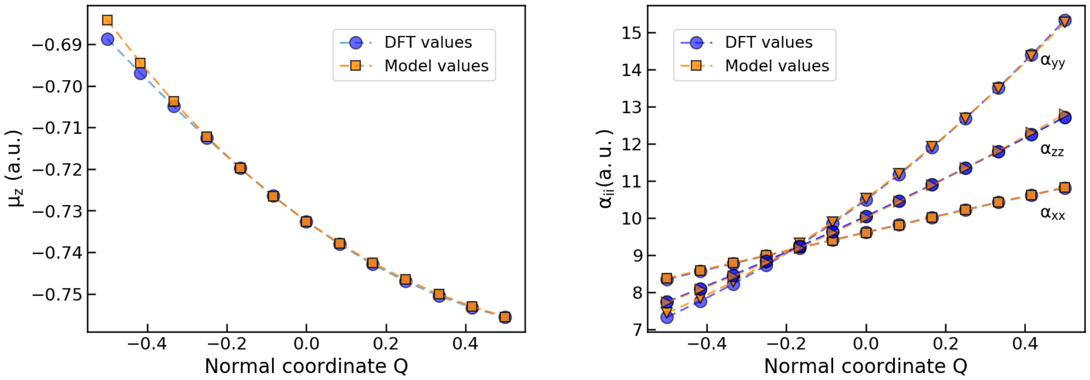

Figure S3: Variation of z-component of molecular dipole (left) and polarizability tensor elements (right) upon displacement of atoms of water molecule in the symmetric bond-stretching mode. The vector of Cartesian atomic displacements was multiplied by the factor Q shown along the x axis.

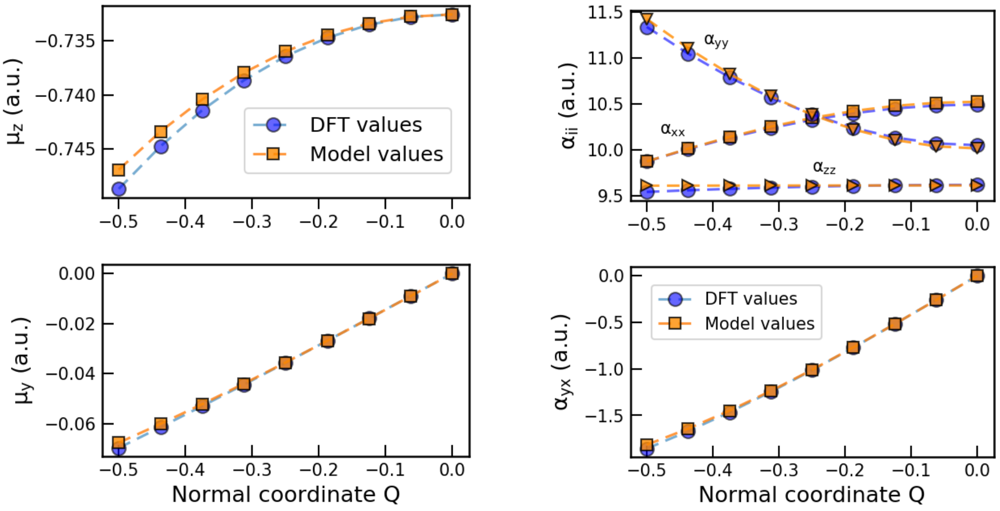

Figure S4: Variation of nonzero components of molecular dipole (left) and of polarizability tensor (right) upon displacement of atoms of water molecule in the asymmetric bond-stretching mode. The vector of Cartesian atomic displacements was multiplied by the factor Q shown along the x axis.

2 Second-order susceptibility calculations

The frequency-dependent $\chi^{(2),R}(\omega)$ tensor was computed using the time correlation function (TCF) formalism.[2,4,5] According to the approach, the pqr element of $\chi^{(2)}(\omega)$ is given by

$$\chi^{(2),R}_{pqr}(\omega) = \frac{i\omega}{k_B T}\int_0^{\infty} dt\, e^{i\omega t}\langle M_r(0)\cdot A_{pq}(t)\rangle, \tag{S19}$$

where M_r and A_{pq} stand for the r and pq components of the system dipole $\mathbf{M}$ and polarizability $\mathbf{A}$, respectively, and k_B is the Boltzmann constant. Making use of (S1) and (S2), the time correlation function in (S19) for the $\chi^{(2),R}_{ssp}$ element reads

$$C_{ssp}(t) \equiv \langle M_p(0)\cdot A_{ss}(t)\rangle = \langle \sum_i \mu_{p,i}(0)\cdot \sum_j a_{ss,j}(t)\rangle. \tag{S20}$$

For a slab of water molecules with the surface plane coinciding with the xy plane and the z-axis perpendicular to the the surface, the ssp element corresponds by the $\chi^{(2)}_{xxz}$ and $\chi^{(2)}_{yyz}$ components and (S20) can be recast to[6–8]

$$C_{ssp}(t) = \langle \sum_i \mu_{z,i}(0)\cdot [a_{xx,i}(t) + a_{yy,i}(t)]\rangle + \langle \sum_i \mu_{z,i}(0)\cdot \sum_{j\neq i}[a_{xx,j}(t) + a_{yy,j}(t)]\rangle, \tag{S21}$$

where the first and second terms in (S21) are intramolecular (self) and intermolecular (cross) parts of the full TCF $C_{ssp}(t)$, respectively. The calculation of the cross TCF in (S21) was performed for molecules j with a mean r_{ij} distance less than 5.5 Å (second minimum in the oxygen-oxygen radial distribution function in bulk liquid water). A contribution of molecules of bulk region to the TCFs (S21) was attenuated[7–9] by multiplying the dipole $\mu_{z,i}(0)$ by a damping function $g(z_i)$

$$\mu'_{z,i}(0) = g(z_i(0))\mu_{z,i}(0), \qquad \text{(S22)}$$

with $z_i(0)$ being the z-coordinate of molecular center-of-mass at $t = 0$; $\mu'_{z,i}(0)$ replaces $\mu_{z,i}(0)$ in (S21). The damping function $g(z)$ has the following form

$$g(z) = \frac{1}{2}\mathrm{sign}(z)\big(\tanh(s(|z| - z_0)) + 1\big), \qquad \text{(S23)}$$

where $g(z_0) = 1/2$ and parameter s determines the width of transition region. Thus, $s = 2.1972$ Å^{-1} gives the width of 1 Å for the $0.1 - 0.9$ region. The sign() function avoids the cancellation of the dipole M_z because of the symmetry of water slab with respect to $z = 0$. By changing z_0, one can select a thickness of interfacial region for the computation of the $\chi^{(2),R}_{ssp}$ susceptibility.

The TCFs were computed on the length $N_c = 2048$ and multiplied by a Hann apodization function of width $N_c/2$ prior to performing the Laplace transform in (S19).

3 Characteristics of silica–water interface with QNULL and QESP parameter sets

Density and orientational order parameter profiles. Figure S5 displays the z-profiles of the relative density ρ^* and of the orientational order parameters S_2 (eqn. (3), main article) computed for the QNULL and QESP surfaces. It is noteworthy that the $S_2(z)$ profiles for the QESP set show an intermediate pattern between the profiles obtained with the QNULL and CLAYFF sets.

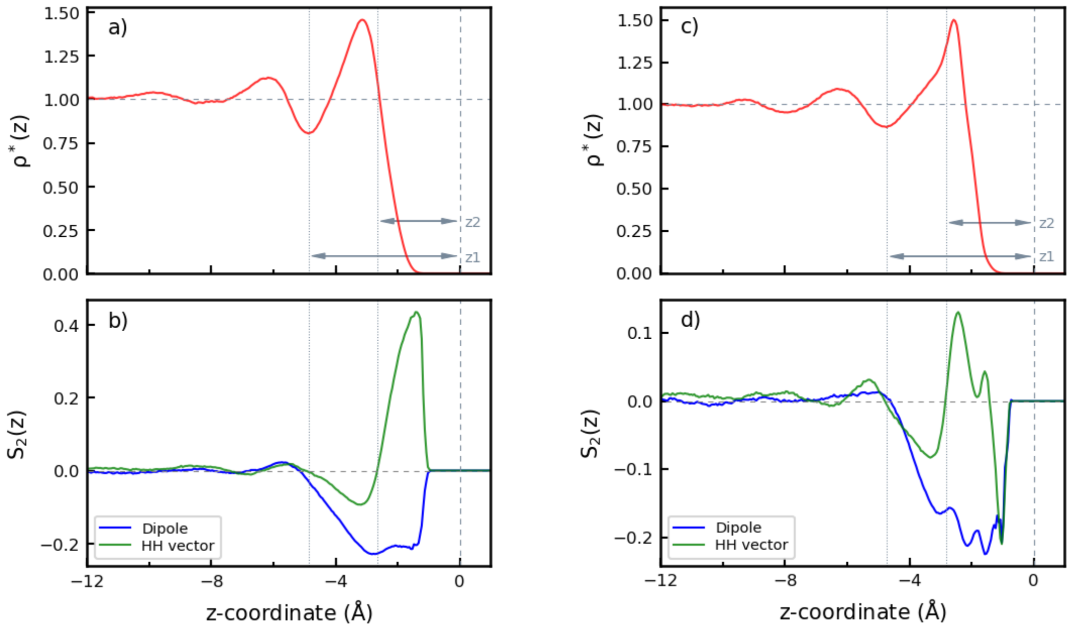

Figure S5: z-profiles of the relative density $\rho^* = \rho/\rho_0$ and of the orientational order parameters $S_2(z)$ of water molecules near the QNULL surface (panels a, b) and QESP surface (panels c, d). The vertical dashed line at $z = 0$ denotes the coordinate of the bottommost silica oxygen atoms taken as the origin of the z-axis; the horizontal dashed line indicates property value characteristic of bulk liquid water. Vertical dotted lines and the corresponding arrows labeled $z1$ and $z2$ are discussed in the text.

Probability density in the surface plane. Figure S6 shows the 2D probability density maps in the *xy* plane for water molecules in the *z*2 region near the QNULL and QESP surfaces (Fig. S5). Note a marked increase of the probability density in the sites A (Fig. 6, main article) with the increase of charges of silica atoms from the QNULL ($q_{\mathrm{Si}} = 0\ |e|$) to QESP ($q_{\mathrm{Si}} = 1.38\ |e|$) sets.

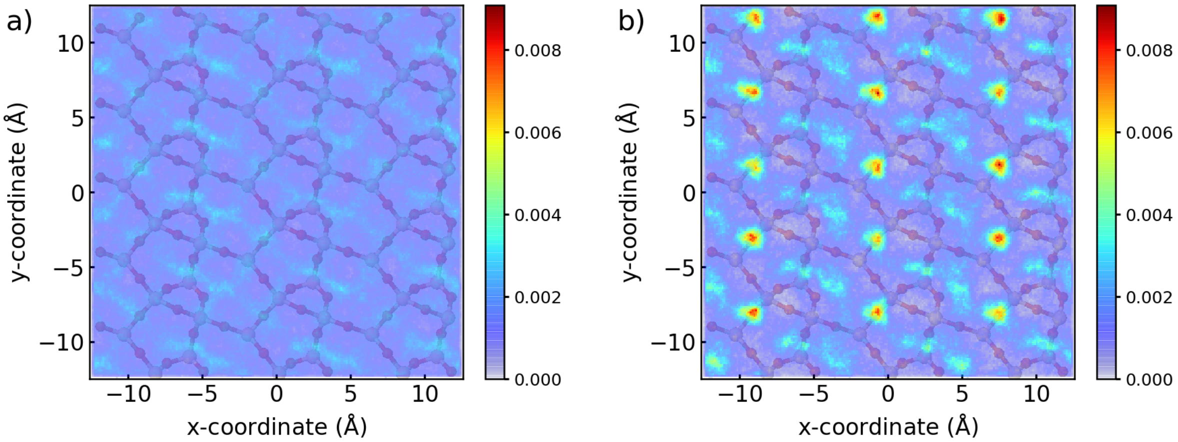

Figure S6: Maps of probability density (in Å^{-2}) for water molecules in the plane parallel to the surface in the *z*2 region; a) – QNULL parameters set, b) – QESP parameters set; the same intensity scale is used for the maps in the panels.

OH bonds orientation.

The probability density maps for the angles ψ between the OH vectors and the *z*-axis for water molecules near the QNULL and QESP surfaces are displayed in Figure S7.

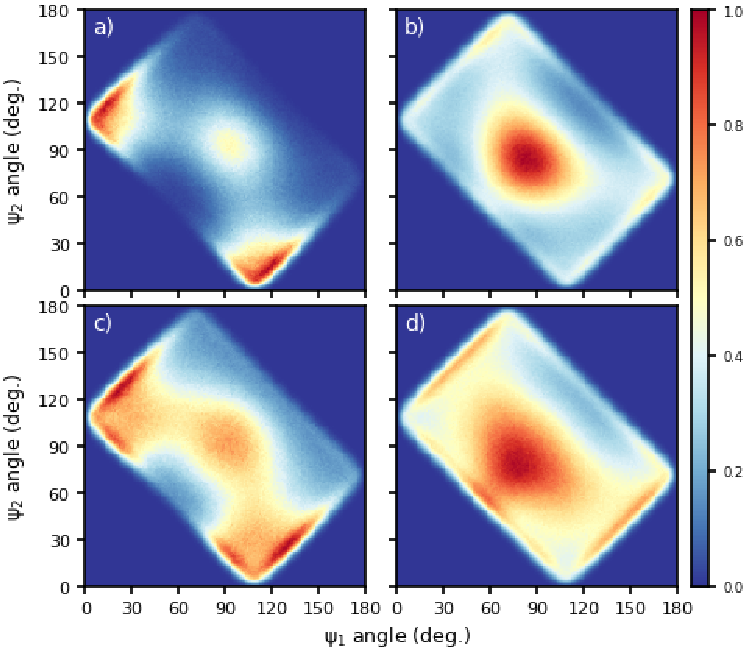

Figure S7: Two-dimensional probability density maps (in arb. units) of the angles ψ between the OH bonds and the *z*-axis for water molecules near the QNULL (a, b) and QESP (c, d) surfaces. Panels a, c – region *z*2; panels b, d – region *z*1, see Fig. S5.

Sum-frequency generation spectra.

Figure S8 presents the Im[$\chi^{(2),R}_{ssp}$] spectra computed for water on the QNULL and QESP surfaces and compares the spectra with the spectrum of water–vapor interface. Note a very similar appearance of the spectra for the

QNULL and water–vapor interfaces with a small downward shift due to weak van der Waals surface-water interactions.

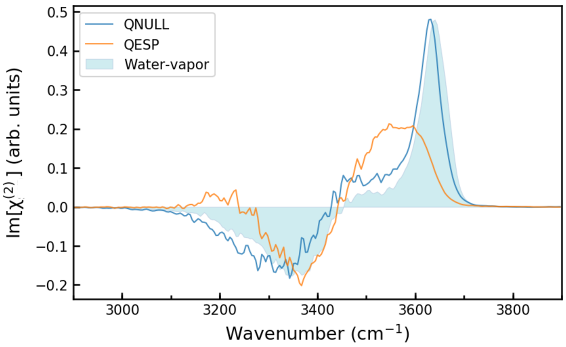

Figure S8: Spectrum of Im[$\chi^{(2),R}$] for the QNULL and QESP silica–water interfaces; the spectrum for water–vapor interface is given for comparison as a filled shape.

Figure S9 displays the dependence of the spectra on the thickness of z-region taken in the calculation of the SFG spectra (parameter z_0 damping function (S23)). For both the hydrophobic surfaces the spectrum of the entire interfacial water is, to a large degree, determined by molecules in the z1-region, the first water layer.

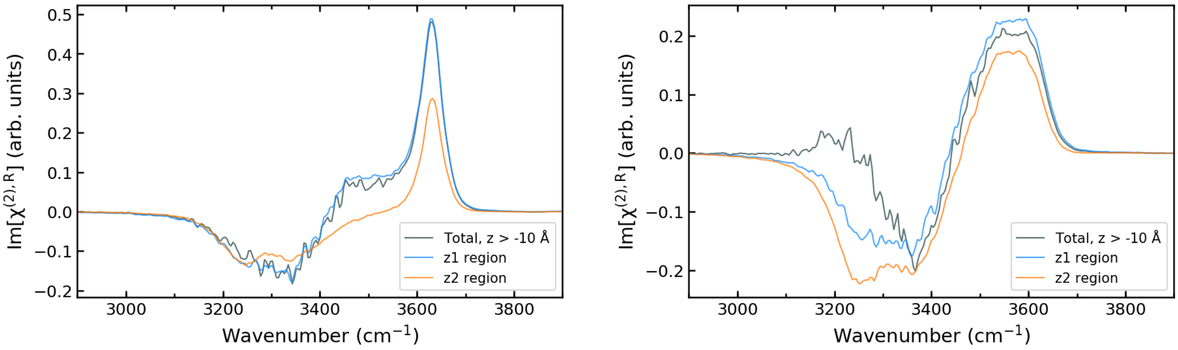

Figure S9: Spectra of Im[$\chi^{(2),R}$] as a function of the distance z from the surface, see Figure S5 for the region definition; left – QNULL surface, right – QESP surface.

4 Water–vapor interface

Results of calculations for the water–vapor interface are reported for the sake of completeness. The simulated system consisted of 500 SPCFw molecules in a slab geometry with the size of the MD simulation box of 25.54 Å along the x and y directions. The calculations were carried out using the same computational protocol as for the interfacial systems (see Section 2.3, main article). Parameters of the damping function (S23) in the SFG spectra calculations were equal $z_0 = 8.0$ and $s = 2.1972$ Å^{-1}.

Density and orientational order parameter profiles.

The calculated $\rho^*(z)$ density profile and the profiles of the orientational order parameters S_2 are shown in Figure S10. The non-zero values of $S_2(z)$ for $z > 4$ Å results from a few molecules escaped the water surface in the course of the simulations.

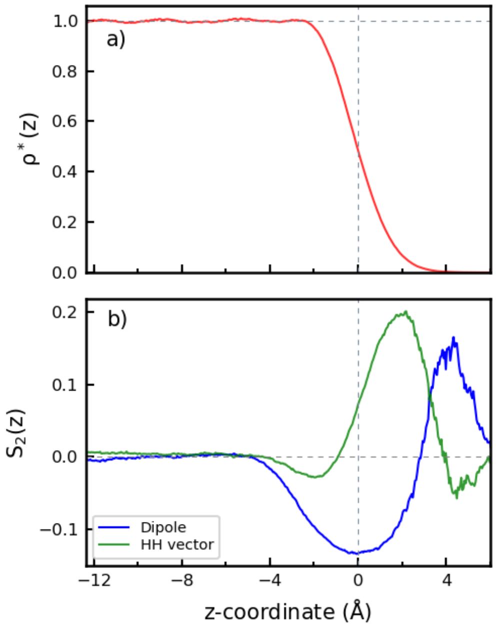

Figure S10: z-profiles of the relative density $\rho^* = \rho/\rho_0$ (a) and of the orientational order parameters $S_2(z)$ (b) of water–vapor interface. The vertical dashed line at $z = 0$ denotes the Gibbs dividing surface; the bulk water side and vapor side are situated in the regions with the negative and positive z values, respectively. The horizontal dashed line indicates property value characteristic of bulk liquid water.

Figure S11 presents the calculated spectra of the imaginary and real parts of the $\chi^{(2),R}_{ssp}$ susceptibility. The spectra are in a good agreement with the results obtained using essentially the same models for the dipole and polarizability of water molecule.[9]

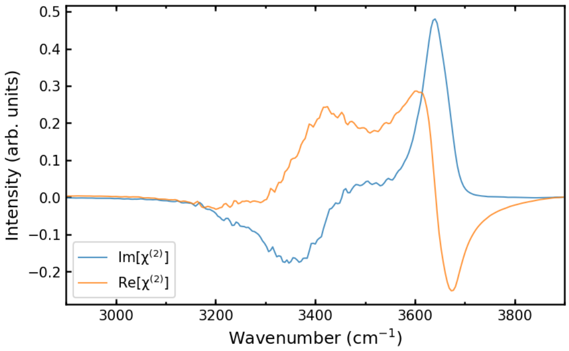

Figure S11: Calculated spectra of the imaginary and real parts of the $\chi^{(2),R}$ nonlinear susceptibility of water–vapor interface.

References

[1] J. Applequist, J. R. Carl and K.-K. Fung, *J. Am. Chem. Soc.*, 1972, **94**, 2952–2960.

[2] A. Morita and J. T. Hynes, *J. Phys. Chem. B*, 2002, **106**, 673–685.

[3] A. J. Sadlej, *Collect. Czech. Chem. Commun.*, 1988, **53**, 1995–2016.

[4] A. Perry, H. Ahlborn, B. Space and P. B. Moore, *J. Chem. Phys.*, 2003, **118**, 8411–8419.

[5] A. Perry, C. Neipert, C. R. Kasprzyk, T. Green, B. Space and P. B. Moore, *J. Chem. Phys.*, 2005, **123**, 144705.

[6] T. Ishiyama and A. Morita, *Chem. Phys. Lett.*, 2006, **431**, 78 – 82.

[7] T. Ishiyama and A. Morita, *J. Phys. Chem. C*, 2007, **111**, 738–748.

[8] Y. Nagata and S. Mukamel, *J. Am. Chem. Soc.*, 2011, **133**, 3276–3279.

[9] A. Morita, *J. Phys. Chem. B*, 2006, **110**, 3158–3163.